Article

pubs.acs.org/Biomac

Biocompatible Glycopolymer Nanocapsules via Inverse Miniemulsion Periphery RAFT Polymerization for the Delivery of Gemcitabine

Robert H. Utama,[‡] Yanyan Jiang,[†,‡] Per B. Zetterlund,*[,†] and Martina H. Stenzel*[,†,‡]

[†]Centre for Advanced Macromolecular Design (CAMD), School of Chemical Engineering, University of New South Wales, Sydney 2052, Australia

[‡]Centre for Advanced Macromolecular Design (CAMD), School of Chemistry, University of New South Wales, Sydney 2052, Australia

Supporting Information

ABSTRACT: Encapsulation of hydrophilic cancer drugs in polymeric nanocapsules was achieved in a one-pot process via the inverse miniemulsion periphery RAFT polymerization (IMEPP) approach. The chosen guest molecule was gemcitabine hydrochloride, which is used as the first-line treatment of pancreatic cancer. The resulting nanocapsules were confirmed to be ~200 nm, with excellent encapsulation (~96%) and loading (~12%) efficiency. Postpolymerization reaction was successfully conducted to create glyocopolymer nanocapsules without any impact on the loads as well as the nanocapsules size or morphology. The loaded nanocapsules were specifically designed to be responsive in a reductive environment. This was confirmed by the successful disintegration of the nanocapsules in the presence of glutathione. The gemcitabine-loaded nanocapsules were tested in vitro against pancreatic cancer cells (AsPC-1), with the results showing an enhancement in the cytotoxicity by two fold due to selective accumulation and release of the nanocapsules within the cells. The results demonstrated the versatility of IMEPP as a tool to synthesize functionalized, loaded-polymeric nanocapsules suitable for drug-delivery application.

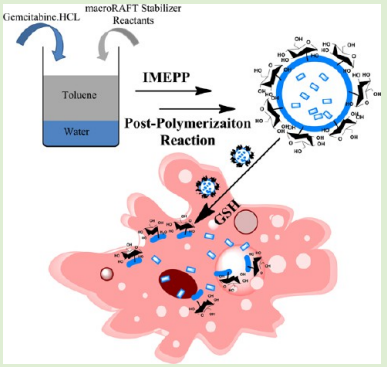

INTRODUCTION

Hollow polymeric nanocapsules have been used extensively to improve the effectiveness of therapeutic agents by increasing their bioavailability and promoting accumulated release within tumor tissues.[1,2] When designing polymeric nanocapsules suitable for delivering therapeutic agents, a range of parameters such as size, shape, and surface characteristics have been reported to greatly affect their efficacy.[3,4] The various synthetic methods to create nanocapsules can be categorized into three different approaches: self-assembly, sacrificial template approaches, and emulsion-based techniques. These methods are all associated with various advantages and disadvantages. For example, self-assembly of amphiphilic molecules allows production of nanocapsules with various shapes, however, with little control over the size and shell thickness,[5,6] while syntheses via sacrificial templates are often tedious but yield excellent control over the size, shape, and shell thickness.[7,8]

Most drug carriers are designed for hydrophobic drugs, where the drug is embedded in a hydrophobic matrix, while the carrier increases the overall solubility of the drug. Drug delivery systems suitable for hydrophilic drugs have gained much interest because the low bioavailability of the drug can be improved by increasing the administered dosage; however, similar to hydrophobic drugs, these drugs still exhibit poor cellular penetration, and they are cytotoxic to both healthy and malignant cells indiscriminately when administrated. Hydrophilic drugs such as peptides or other low-molecular-weight hydrophilic drugs have different demands in regards to a suitable drug carrier because the drug cannot easily be encapsulated in a compatible polymer matrix.[9] An example of a water-soluble anticancer drug is gemcitabine, which has recently been approved by the FDA for treatment of a range of cancers, in particular, the inherently difficult to treat pancreatic cancer. Commercially available gemcitabine, which comes in its hydrophilic salt form, is currently administrated at a relatively high dosage (1000 mg/m^2) to compensate for its very short plasma life (8−17 min).[10] Furthermore, application of drug delivery systems with gemcitabine is currently still limited but already showing excellent potential in improving the cytotoxicity toward cancer cells.

Conjugation of a hydrophilic moiety to gemcitabine represents one pathway to improve the blood circulation time and stability of gemcitabine. Hydrophilic polymers such as poly(ethylene glycol) (PEG)[11] have been confirmed to improve the bioavailability of the drug. Furthermore, various functionalities have been successfully exploited to introduce certain release mechanisms[12] and targeting characteristics[13,14] onto the polymeric−drug conjugate. Such conjugates have also been successfully self-assembled to produce polymeric micelles to protect the load from degradation, thus improving its

Received: April 22, 2015
Revised: May 22, 2015
Published: May 31, 2015

DOI: 10.1021/acs.biomac.5b00545
Biomacromolecules 2015, 16, 2144−2156

Scheme 1. Schematic Illustrating the Synthesis of Loaded Nanocapsules Having Reducible Shells via IMEPP

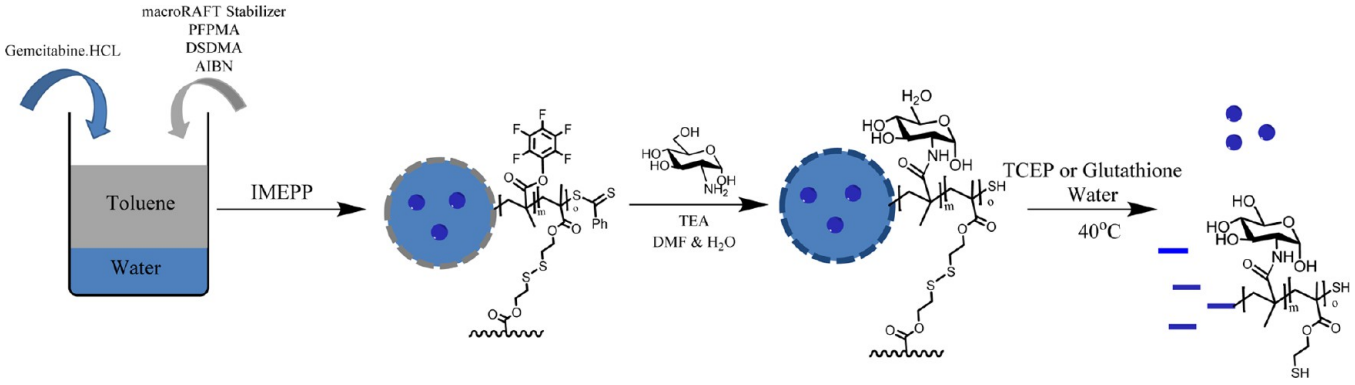

stability;[15,16] however, the pertaining issues with the quantity of polymers used, low loading efficiency and the inefficient release of the drug, make this particular approach rather inferior to other drug-delivery systems.

In contrast, physical encapsulation offers better loading efficiency while still maintaining all of the benefits of using drug delivery systems previously mentioned; however, gemcitabine has been reported to readily diffuse out under physiological conditions, hence causing low encapsulation efficiencies and rapid release rates.[17] Both Haam and coworkers[18] and Couvreur and coworkers[19] encapsulated gemcitabine in polymeric nanospheres using emulsion polymerization. The results of their study confirmed the rapid release rate of gemcitabine. Low loading efficiency was reported in both cases (7.4 and 4%, respectively), which is a characteristic of nanospheres as a drug delivery system. The use of liposomes (which mimic the morphology of nanocapsules) to deliver gemcitabine was demonstrated by Fresta and coworkers.[20,21] The results were promising with better loading efficiency (~13−29%) than using nanospheres as well as enhanced antitumor activity to that of free gemcitabine. In liposomes, however, high loading efficiency comes at the expense of thin polymeric membrane shells. Moreover, hydrophilic moieties encapsulated in liposomes have been found to be localized in the aqueous region close to the membrane bilayer.[22] The combination of these two factors leads to rapid release of the drugs upon application, thus eliminating the advantages of using a drug-delivery system.

Amphiphilic gemcitabine derivatives have been developed and utilized with micellar or liposomal delivery systems to potentially overcome the inherent issues with encapsulating gemcitabine, especially related to the rapid release of the drug. Mixed results, however, were reported from these experiments. First of all, the commonly used prodrug derivative carrying a stearoyl chain (GemC18) was reported to show both higher[10] and lower[23] cytotoxicity than the native gemcitabine. The application of liposomes offered greater loading efficiency than micelles, although encapsulation in micelles was found to improve the cytotoxicity of the prodrug,[23,24] while loaded liposomes did not show an improvement in cytotoxicity.[10,25] Excellent results in terms of biological activity were obtained by conjugation of gemcitabine to polymers,[26−31] where the release of the drug was delayed by the additional scission step.

The use of emulsion approaches to produce polymeric nanocapsules has to date been strongly focused on miniemulsions, whereby nanodroplet templates are produced in the size range of 50−500 nm. The size of the droplets, and hence the resulting nanocapsules, can be controlled by varying the miniemulsion conditions such as the quantity of surfactants or dispersed phase, while the drug can be simultaneously entrapped in a one-pot process.[32−34] Moreover, this process can be combined with various polymerization techniques to allow the production of shells with well-controlled porosity as well as surface characteristics;[35−38] however, there are still limitations with the currently available methods, for example, the generation of solid nanospheres[39,40] or the use of nonbiocompatible surfactants.[41] We have previously reported inverse miniemulsion periphery RAFT polymerization (IMEPP), which completely eliminates the need of surfactant as well as formation of solid nanospheres.[42] IMEPP creates polymeric shells by RAFT polymerization, which is initiated and growing from the outer surface. Therefore, IMEPP offers excellent control over the shell thickness, porosity, as well as surface characteristic.[43,44] The core reservoir of the resulting nanocapsules is designed to be reaction free (i.e., polymerization does not occur inside particles), and as such the use of IMEPP ensures there is no chemical degradation of the hydrophilic loads.[45]

Despite the advancements in recent years in the field of nanocapsule synthesis, the number of reports on the use of nanocapsules to deliver water-soluble drugs is limited, although this pathway offers the clear advantages of potentially high encapsulation efficiencies as well as the delivery of drugs in their preferred environment. An example of the use of nanocapsules to deliver gemcitabine hydrochloride was reported by Paolino and coworkers, who used a double-emulsion to produce loaded-PLA nanocapsules of ~200 nm[46] with ~90% encapsulation efficiency (EE) and ~1.33% loading efficiency. The release of the loads was found to be slow, reaching 40% after 24 h, in contrast with the liposomal system[20] previously described. Improvement in gemcitabine cytotoxicity was also observed when using the nanocapsules, despite the low loading efficiency.

Herein, we report the synthesis of gemcitabine-loaded nanocapsules using the IMEPP process. Functional block copolymers based on the biocompatible poly(*N*-(2-hydroxypropyl)methacrylamide) (PHPMA) and the reactive pentafluorophenyl methacrylate were synthesized via RAFT polymerization. Nanodroplet templates encapsulating gemcitabine were obtained using inverse miniemulsions stabilized by block copolymers. The presence of RAFT functionalities allows controlled/living polymerization and cross-linking to be conducted, while the highly active pentafluorophenyl functionality on the shell offers the opportunity to modify the shell of

DOI: 10.1021/acs.biomac.5b00545
Biomacromolecules 2015, 16, 2144−2156

the nanocapsules with biocompatible functionalities such as carbohydrates, while enabling simultaneous cross-linking (Scheme 1). The cytotoxicity of the resulting loaded-nanocapsules was tested against pancreatic cancer cells and compared with that of free gemcitabine hydrochloride.

EXPERIMENTAL PART

Materials. *N*-(2-Hydroxypropyl) methacrylamide (HPMA, Polysciences), D-(+)-glucosamine hydrochloride (≥99%, Sigma-Aldrich), triethylamine (≥99%, Sigma-Aldrich), methacryloyl chloride (≥97%, Fluka), sodium hydrogen carbonate (Na_2CO_3, Univar), sodium chloride (NaCl, Univar), magnesium sulfate ($MgSO_4$, Univar) pentafluorophenol (≥99%, ChemImpex), toluene (99.5%, Univar), *N*,*N*-dimethylacetamide (DMAc, 99.9%, Sigma-Aldrich), diethyl ether (Et_2O, 99%, Univar), methanol (Ajax Chemicals), tetrahydrofuran (THF, anhydrous, 98%, Sigma-Aldrich), anhydrous dichloromethane (>98%, Sigma-Aldrich), *N*,*N*-dimethylformamide (DMF, >99.8%, Sigma-Aldrich), 1,4-dioxane (99.5%, Sigma-Aldrich), *n*-hexane (95%, Univar), and silica gel (Grace) were used as received. Deuterated NMR solvents ($CDCl_3$, DMSO, and D_2O) were purchased from Cambridge Isotope Laboratories. Ethylene glycol dimethacrylate (EGDMA, 98%, Sigma-Aldrich) was deinhibited by passing through a column of activated basic alumina. Deinhibited monomers were stored at <4 °C and used within 7 days. 2,2′-Azobis(isobutyronitrile) (AIBN) was recrystallized twice from methanol. Deionized (DI) water was produced by a Milli-Q reverse osmosis system and had a resistivity of 19.6 mΩ cm^{-1}. The RAFT agent, 4-cyanopentanoic acid dithiobenzoate (CPADB), was synthesized according to the literature.[47]

Analyses. *Size Exclusion Chromatography.* Size exclusion chromatography (SEC) was performed using a Shimadzu modular system, comprising an SIL-10AD autoinjector, LC-10AT pump, a DGU-12A degasser, CTO-10A column oven, and an RID-10A differential refractive index detector. A column arrangement consisting of a Polymer Laboratories 5.0 μm bead size guard column (50 × 7.8 mm), followed by four linear PL column (300 × 7.8 mm; 500, 10^3, 10^4, and 10^5 Å; 5 μm pore size) was used for the analysis. *N*,*N*-Dimethylacetamide (DMAc, 0.03% w/v LiBr, 0.05% w/v 2,6-dibutyl-4-methylphenol (BHT)) was used as the mobile phase at a constant temperature of 50 °C and a constant flow rate of 1 mL·min^{-1}. The SEC system was calibrated using linear polystyrene standards, ranging from 500 to 10^6 g/mol (Polymer Laboratories). Chromatograms were processed using Cirrus 2.0 software (Polymer Laboratories).

Nuclear Magnetic Resonance. Nuclear magnetic resonance (NMR) was utilized to analyze the structure of the synthesized compounds as well as to determine the monomer conversion. ^{1}H NMR spectroscopy was carried out using a Bruker Avance III 300, equipped with an auto sampler system, and 600 MHz, equipped with a cryoprobe. Chemical shifts are reported in parts per million (ppm), relative to the residual solvent peak. The theoretical molecular weight ($M_{n,th}$) was calculated according to the following equation

$$M_{n,th} = \frac{[\text{monomer}]}{[\text{RAFT}]} \times \text{conversion} \times M_{\text{monomer}} + M_{\text{RAFT}} \quad (1)$$

M_{RAFT} stands for the molecular weight of the RAFT agent or the macroRAFT agent

Dynamic Light Scattering. Dynamic light scattering (DLS) analyses were run on a Zetasizer Nano ZS (Malvern) with a 4 mV He−Ne laser operating at λ = 632 nm and noninvasive backscatter detection at 173°. Measurements were conducted in a Quartz cuvette at 25 °C, with 30 s equilibration period prior to each set of measurements. For a given sample, a total of three measurements were conducted. In each measurement, the number of runs, attenuator, and path length used were automatically adjusted by the instrument, depending on the quality of the sample. The presented results are averages of the three measurements.

Fourier Transform Infrared Spectroscopy. Fourier transform infrared spectroscopy spectra were obtained using Bruker Spectrum BX FTIR system using diffuse reflectance sampling accessories.

High-Performance Liquid Chromatography. The high-performance liquid chromatography (HPLC) system comprised a LC-20AD pump, DGU-20A degasser, CTO-20A oven (30 °C), and SPD-20A UV−vis detector. Resteck C18 column (5.0 μm bead sizes, 250 × 4.60 mm) was used in all measurements. All samples were prepared in DI water and filtered through a 0.45 μm syringe filter. The mobile phase was a mixture of methanol (40% v/v) and water, operating at a flow rate of 1 mL min^{-1}. Analysis was carried out at 270 nm wavelength, with the maximum peak at 3.3 min retention time corresponding to the gemcitabine hydrochloride.

Cryo-Transmission Electron Microscopy. Cryo-transmission electron microscopy (Cryo-TEM) micrographs were obtained according to the following procedure. A sample droplet of 2 μL was put on a lacey carbon-film-covered copper grid (Science Services, Munich, Germany or Quantifoil S7/2, Micro Tools, Jena, Germany), which was hydrophilized by glow discharge for 30 s. Most of the liquid was then removed with blotting paper, leaving a thin film stretched over the lace holes. The specimens were instantly shock-frozen by rapid immersion into liquid ethane and cooled to ∼90 K by liquid nitrogen in a temperature-controlled freezing unit (Carl Zeiss Microscopy, Jena, Germany). The temperature was monitored and kept constant in the chamber during all sample preparation steps. After the specimens were frozen, the remaining ethane was removed using blotting paper. The specimen was inserted into a cryo transfer holder (CT3500, Gatan, Munich, Germany) and transferred to a Zeiss/LEO EM922 Omega energy-filtered TEM (EFTEM) instrument (Carl Zeiss Microscopy). Examinations were carried out at temperatures around 90 K. The TEM instrument was operated at an acceleration voltage of 200 kV. Zero-loss-filtered images (ΔE = 0 eV) were taken under reduced dose conditions (100−1000 e/nm^2). All images were recorded digitally by a bottom-mounted charge-coupled device (CCD) camera system (Ultra Scan 1000, Gatan, Munich, Germany) and combined and processed with a digital imaging processing system (Digital Micrograph GMS 1.8, Gatan, Munich, Germany).

Transmission Electron Microscopy. Transmission electron microscopy (TEM) was conducted using a JEOL1400 TEM operating at an accelerating voltage of 120 kV. Images were recorded via the Gatan CCD imaging software. All TEM samples were prepared by dropping a 1 mg mL^{-1} emulsion on a Formvar supported copper grid. Excess solvent was drained using filter paper after 1 min.

Synthesis of Pentafluorophenyl Methacrylate (PFPMA). Pentafluorophenol (19.37 g, 0.10 mol) and 15 mL of TEA (0.10 mol) were dissolved in 200 mL of anhydrous DCM and placed in a 0 °C ice bath. Methacryloyl chloride (10 g, 0.09 mol) was added dropwise. After the addition, the mixture was then stirred overnight at room temperature, followed by filtration of the precipitated salt. The solution was then washed twice with Na_2CO_3 and twice with distilled water, followed by drying over $MgSO_4$. The solvent was then removed, and the remaining mixture was then distilled under reduced pressure to yield a colorless product (16.4 g, 68%).

Synthesis of Bis(2-methacryloyloxyethyl) Disulfide (DSDMA). 2-Hydroxyethyl disulfide (12.5 g, 0.081 mol) and triethylamine (24.5 g, 0.242 mol) were mixed together in 250 mL of anhydrous dichloromethane. The solution was then purged with nitrogen for 15 min and placed in a 0 °C ice bath. Methacryloyl chloride (34 g, 0.325 mol) was added dropwise into the reaction mixture, while still maintaining the 0 °C condition. After the addition, the solution was brought up into room temperature and further stirred for 24 h. The resulting salt was then filtered, and the mixture was washed twice with DI water, twice with Na_2CO_3, and finally twice with brine. The mixture was dried over $MgSO_4$. Excess solvent was then removed, and the remaining mixture was columned using silica gel as the stationary phase and chloroform as the eluent. Pale-yellow oil was obtained after removing the volatiles (15.69 g, 67%).

Synthesis of Poly(*N*-(2-hydroxypropyl methacrylamide)) (PHPMA) macroRAFT Agent. HPMA (1 g, 6.984 × 10^{-3} mol), CPADB (0.049 g, 1.74 × 10^{-4} mol) as RAFT agent, and AIBN (0.006

DOI: 10.1021/acs.biomac.5b00545
Biomacromolecules 2015, 16, 2144−2156

Scheme 2. Schematic Pathway for the Synthesis of the macroRAFT Stabilizer

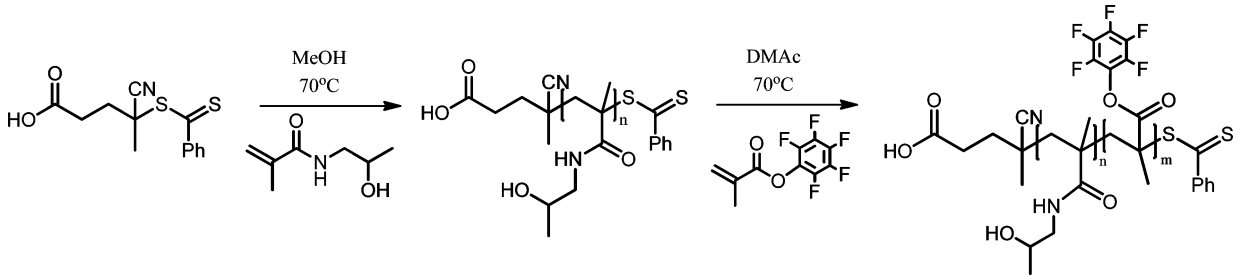

g, 3.49×10^{-5} mol) as initiator were dissolved in methanol (6.98 mL) to give a [monomer]:[RAFT]:[initiator] ratio of 40:1:0.2. The solution was thoroughly purged with nitrogen gas for 30 min while immersed in an ice bath. The solution was placed in a preheated oil bath at 70 °C for 7 h. After polymerization, the reaction was stopped by placing the solution in an ice bath. The polymer was isolated by precipitation in diethyl ether to yield PHPMA as a highly viscous red liquid. The monomer conversion was determined to be 38% via ^{1}H NMR. ($M_{n,th}$ = 2500 g mol^{-1}, $M_{n,SEC}$ = 5300 g mol^{-1} (with respect to PS standards), $Đ$ = 1.12).

Synthesis of Poly(*N*-(2-hydroxypropyl methacrylamide))-*b*-poly(pentafluorophenyl methacrylate) (PHPMA-*b*-PPFPMA) macroRAFT Stabilizer. P(HPMA) (0.2 g, 8×10^{-5} mol) was employed as macroRAFT agent and mixed with PFPMA (1.00 g, 4×10^{-3} mol) and AIBN (2.62 mg, 1.6×10^{-5} mol) in DMAc (2 mL) to give a [monomer]:[macroRAFT]:[initiator] ratio of 50:1:0.2. The solution was thoroughly degassed in an ice bath for 30 min before being placed in an oil bath at 70 °C for 6 h. The polymerization was stopped by placing the solution in an ice bath for 30 min. The final solution was then precipitated in hexane to yield a brittle, pink solid. The monomer conversion was 71% determined by ^{19}F NMR. ($M_{n,th}$ = 11 500 g mol^{-1}, $M_{n,SEC}$ = 16 200 g mol^{-1} (with respect to PS standards), $Đ$ = 1.18).

Synthesis of Empty and Loaded Nanocapsules via Inverse Miniemulsion Periphery RAFT Polymerization (IMEPP). Toluene was mixed with the macroRAFT stabilizer, EGDMA or DSDMA (cross-linker), PFPMA (monomer), and AIBN (initiator) in a 25 mL glass bottle to create the continuous (organic) phase. In a separate container, DI water and lipophobe were mixed to create the dispersed phase and subsequently added to the organic phase. For the loaded nanocapsules, gemcitabine hydrochloride was dissolved in the dispersed phase prior to the addition. The mixture was then sonicated (Branson 450 sonifier, 55% amplitude, 5 mm tip diameter) for 5 min. The resulting miniemulsion was transferred into glass ampules to undergo repeated cycles of nitrogen purging/evacuation. The ampule was subsequently flame-sealed under vacuum. Polymerization was then carried out at 70 °C with constant shaking in an oil bath for 7 h. Nanocapsules were collected from the raw emulsion by de-emulsifying the system using hexane, followed by centrifugation (7000 rpm for 5 min) and drying under reduced pressure at 40 °C.

Aminolysis of the Activated Ester Group by D-(+)-Glucosamine. The previously prepared nanocapsules were initially dispersed in DMF and TEA solution using the sonication bath. A second solution was prepared comprising D-(+)-glucosamine in Na_2CO_3 solution (pH 11) and added dropwise under constant stirring into the dispersion. The reaction was carried out in a preheated oil bath at 40 °C under constant stirring for 8 h. At the completion of the reaction, the solution was dialyzed against Na_2CO_3 solution for 1 day and lyophilized.

Quantification and Release Experiments of GEM. Initially, a calibration curve was constructed. Pure GEM solution (10 μL) at various concentrations (0.01 to 1 mg/mL) was analyzed using a UV detector at 270 nm wavelength. It was found that the peak corresponding to the drug was produced after 3.3 min. Two solutions (5 mL) of the nanocapsules with sugar shell dispersed in water (0.5 mg/mL) were prepared. Into the first solution, TCEP was added and the reaction was stirred for 1 h at 40 °C. For the second solution, it was stirred in Na_2CO_3 solution (pH 11) over the period of 24 h, with samples taken out after 5, 12, 24, and 48 h. Each solution was filtered through 0.45 μm syringe filter, before being analyzed via HPLC. The area under the signal corresponding to the GEM was collected for each sample and used to calculate the amount of GEM released.

The EE is calculated using the following formula

$$\mathrm{EE}(\%) = \frac{\text{mass of gemcitabine used}}{\text{mass of gemcitabine recovered}} \times 100 \quad (2)$$

While the loading efficiency (LE) is calculated according to

$$\mathrm{LE}(\%) = \frac{\text{mass of gemcitabine recovered}}{\text{mass of polymeric nanocapsules}} \times 100 \quad (3)$$

In Vitro Cell Culture. Human pancreatic carcinoma (AsPC-1) cells were cultured in T 25 tissue culture flasks with RPMI 1640 medium supplemented with 10% fetal bovine serum at 37 °C under an atmosphere of 5% CO_2. After reaching the desired confluence, the cells were collected by trypsin/EDTA treatment. The cells were then used for the subsequent growth inhibition studies.

Growth Inhibition Studies. AsPC-1 cells were seeded in 96-well cell culture plates at 4000 cells/well at 37 °C for 24 h. All four samples (GEM, G-RNP, G-SNP, and RNP) were sterilized by UV irradiation for 20 min and then serially diluted (2× dilution factor) with sterile Milli-Q water. The medium in the cell culture plate was discarded and replaced with 100 μL of fresh, twice-concentrated RPMI 1640 serum medium. The cells were incubated with the nanocapsules for 72 h. The culture medium was then discarded, and 100 μL of 10% TCA was added to each well, followed by incubation of the plates for 45 min at 4 °C. The supernatant was discarded, and the plates were washed five times with water and air-dried. 100 μL of 0.4% (w/v) SRB solution in 1% acetic acid was added to each well, and the plates were incubated for 20 min at room temperature. After staining, the unbound dye was removed by washing (five times) with 1% acetic acid, followed by air-drying of the plates. Bound stains were solubilized with 200 μL of 10 mM tris buffer, and the absorbance was measured using Bio-Rad BenchMark microplate reader (λ = 490 nm). The resulting data were then analyzed and plotted using GraphPad Prism 6.0.

RESULTS AND DISCUSSION

Synthesis of the macroRAFT Stabilizer. The amphiphilic block copolymer was synthesized via RAFT polymerization to give control over the number of repeating unit as well as to introduce RAFT functionality for the subsequent IMEPP. PHPMA with 16 repeating units (determined from ^{1}H NMR) was chosen for the hydrophilic segment due to its biocompatibility, stability, and excellent hydrophilicity.[48] The resulting macroRAFT agent was chain extended with PFPMA having 36 repeating units. This was determined from ^{19}F NMR by comparing the fluorine signal in the p position of both monomer (−158.7 ppm) and polymer (−156.8 ppm). The introduction of the activated ester group was necessary for the postpolymerization modification reaction of the nanocapsule shells. The calculated hydrophilic−lipophilic balance HLB value

DOI: 10.1021/acs.biomac.5b00545
Biomacromolecules 2015, 16, 2144−2156

for the block copolymer was 4.35, determined using the equation previously described,[42] making it suitable as stabilizer for an inverse miniemulsion system.

NMR spectroscopy was used to confirm the structure of both the homo and block copolymers (Figure S1 in the SI). ^{19}F-NMR (Figure S1 in the SI, top) of the block copolymer confirmed the presence of the PFPMA block. The splitting of the fluorine signal at the ortho position is a characteristic of the polymerized PFPMA, caused by the slight alteration in the chemical environment due to the methyl group of the polymeric backbone. SEC analysis of the macroRAFT and the block copolymer (Figure 1) gave number-average molecular weights (M_n) of 5300 and 16 200 g·mol^{-1}, respectively. The polydispersity ($Đ$) of both polymers was <1.2, indicating good control/livingness, with $Đ$ of the block copolymer being slightly higher due to some low-molecular-weight tailing.

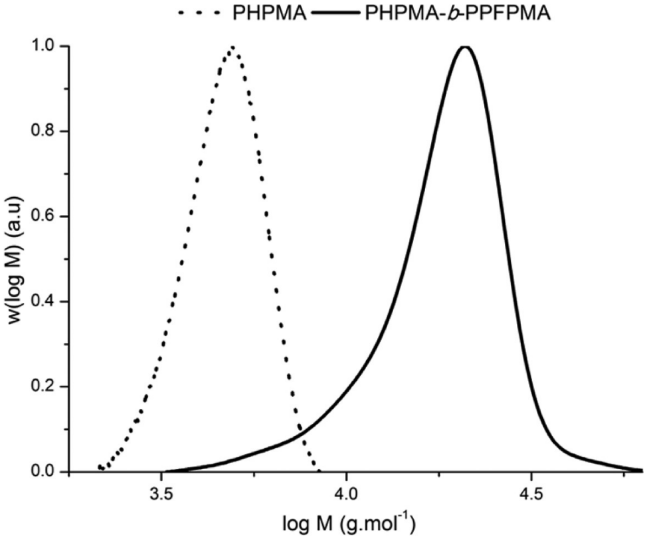

Figure 1. Molecular weight distributions of the macroRAFT agent (dotted, $Đ$ = 1.12) and the amphiphilic block copolymer stabilizer (solid, $Đ$ = 1.18).

Synthesis of Hollow and Loaded Nanocapsules via IMEPP. Hollow polymeric nanocapsules were synthesized according to the previously described method by our group.[42] IMEPP relies on an amphiphilic block copolymer to serve as both stabilizer and to interfacially confine the subsequent RAFT polymerization to the continuous phase (i.e., chains grow outward from the water−oil interface). The previously synthesized PHPMA-*b*-PPFPMA was used as the stabilizer for all of the presented experiments. A relatively high stabilizer content (30 wt % rel. dispersed phase) was utilized to obtain a more compact shell, in contrast with our previously synthesized nanocapsules, which allowed a rather large molecule (BSA) to diffuse out.[45] The inverse miniemulsion recipe used is summarized in Table 1. The initial diameter (d_i) of the droplets was established to be 216 nm (PDI = 0.04).

The initial miniemulsion (prior to polymerization) was visualized using cryo-TEM (Figure 2). Analysis of the micrographs showed that the droplets had an average diameter in the range 168−194 nm, which is in accordance with the DLS result (217 nm). Closer inspection of the periphery of the droplets revealed the presence of the polymeric layer (PPFPMA, ∼6 nm thick), which produced a stronger contrast than the aqueous core.

The role of the lipophobe (NaCl) in an inverse miniemulsion is to prevent Ostwald ripening.[49] Typically, low-molecular-weight ionic salts are found to be suitable. The drug of interest, gemcitabine hydrochloride (GEM·HCl), comes in a salt form and has excellent solubility in water and negligible solubility in toluene. Because of its similarity to common lipophobes used, the suitability of GEM·HCl as lipophobe (and guest molecule) was investigated. The size and stability of the initial miniemulsion obtained were then compared with the typical inverse miniemulsion with NaCl as the lipophobe.

The two inverse miniemulsion recipes used are summarized in Table 1. In both cases, the molar concentration of salts in water was kept very similar (0.296 mM for NaCl and 0.292 mM for GEM·HCl). To fully solubilize GEM·HCl in water at the desired concentration, we employed mild heating and sonication. Upon sonication, both inverse miniemulsions showed similar milky characteristics. DLS analysis yielded d_i = 224 nm with a narrow droplet size distribution index (PDI) of 0.04. Complete encapsulation of the GEM in the dispersed phase was also confirmed from the DLS data, as no precipitate could be detected in the intensity distribution plot (which would be represented by peaks in the micron range), as gemcitabine hydrochloride is not soluble in toluene. The system was stable with no visible-phase separation and significant changes in droplets characteristics after 2 days. Therefore, GEM·HCl was confirmed to be suitable, as lipophobe as the system costabilized by GEM·HCl behaved in the same way as the system costabilized by NaCl.

The miniemulsion system is relatively stable under the current conditions but would eventually degrade with time or upon drying or exposure to environmental changes in temperature or solvent. To permanently stabilize these nanocapsules, we carried out cross-linking by chain extension of the block copolymer in the presence of divinyl cross-linkers. Four different nanocapsules were synthesized: nanocapsules having permanent (EGDMA) and reducible (DSDMA) polymeric shells, referred to as SNP and RNP, respectively, and their corresponding GEM-loaded counterparts (G-SNP and G-RNP).

From the FTIR analysis (Figure 3) on the purified nanocapsules, the appearance of the carbonyl ester (PEGDMA or PDSDMA, 1719 cm^{-1}) peak confirmed the success of the

Table 1. Inverse Miniemulsion Recipe Used to Synthesize Empty Nanocapsules and Gemcitabine-Loaded Nanocapsules

cont. phase	disp. phase	hollow NPs	GEM NPs	comment
toluene (g)		8.667		
stabilizer (g)		0.260		30 wt % rel. water
	water (g)	0.867		10 wt % rel. toluene
	NaCl (g, mmol)	0.017, 0.296		2 wt % rel. water
	GEM·HCl (g, mmol)		0.087, 0.292	10 wt % rel. water
ultrasonication (time, amplitude, power)			5 min, 55%, 450 W	

DOI: 10.1021/acs.biomac.5b00545
Biomacromolecules 2015, 16, 2144−2156

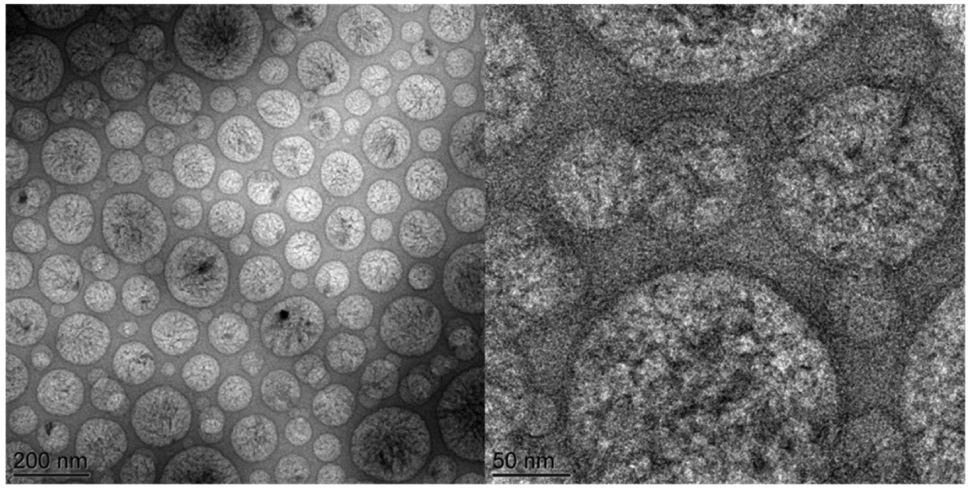

Figure 2. Cryo-TEM micrographs of the inverse miniemulsion stabilized by the amphiphilic PHMA-*b*-PPFPMA, with the darker regions around the droplets corresponding to the amphiphilic block copolymers behaving as stabilizers.

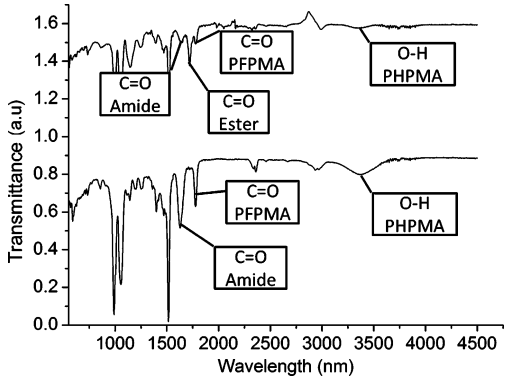

Figure 3. FTIR spectrum of the PHPMA-*b*-PPFPMA (bottom) and the nanocapsules (SNP, top), showing the appearance of the C═O ester peak corresponding to the cross-linker used.

cross-linking. Furthermore, the signals from the HPMA (amide and OH) were weakened due to the relatively lower concentration of this polymer in the final product. The resulting nanocapsules were redispersed in various solvents to confirm their stability even after purification. Monomodal distributions (Figure 4 and Figure S2 in the SI) were obtained in all cases with a PDI of 0.2 or less. DLS analysis of the dispersion in toluene gave d_i = 280 and 266 nm (respectively, for SNP and RNP), which was comparable to the initial droplet size before polymerization. Furthermore, the integrity of the shell was confirmed by redispersion of the purified nanocapsules in DMAc. This solvent was chosen because it is a good solvent for both PHPMA and PPFPMA; therefore, chains that are not cross-linked would dissolve, presumably resulting in smaller or wholly/partially disintegrated, nanocapsules.

As the suitability of GEM as lipophobe was successfully confirmed, this recipe was then used to synthesize GEM-loaded nanocapsules. Polymerizations were conducted with both EGDMA and DSDMA as cross-linking agents (Table 2). DLS analyses were also conducted on these samples, with the results indicating successful production of stable loaded-polymeric nanocapsules (Table 3). The monomodal distribution of the redispersed nanocapsules in toluene confirmed the successful encapsulation of GEM·HCL, while nanocapsule redispersion in DMAc confirmed the shell integrity.

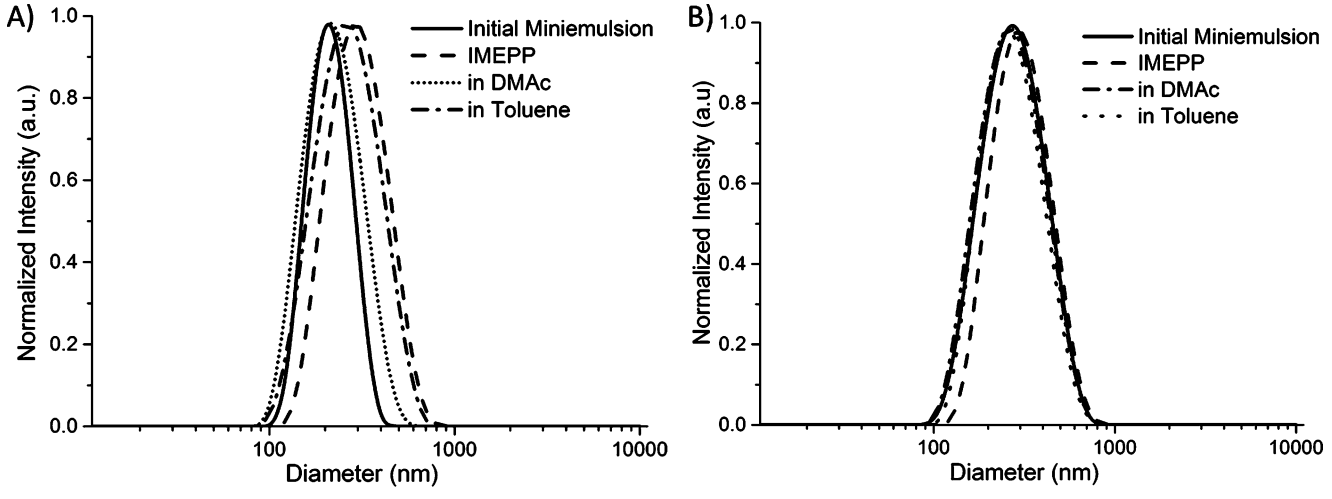

Figure 4. Intensity-based distribution (normalized to 1) showing the initial droplets, the final product prior to purification (IMEPP), and the purified nanocapsules redispersed in toluene and in DMAc of SNP (A) and G-SNP (B).

DOI: 10.1021/acs.biomac.5b00545
Biomacromolecules 2015, 16, 2144−2156

Table 2. IMEPP Parameters for Synthesis of Polymeric Nanocapsules with PFPMA and Either EGDMA (permanent) or DSDMA (reducible) Shell

parameter	permanent NPs	reducible NPs	comment
PHPMA-*b*-PPFPMA (g)	0.260	0.260	[M]:[CL]:[RAFT]:[AIBN] = 100:50:1:0.5
PFPMA (g)	0.299	0.299	
EGDMA (g)	0.235		
DSDMA (g)		0.344	
AIBN (mg)	2.3	2.3	
conversion (hollow, %)	71	72	
conversion (loaded, %)	69	70	
polymerization time (h)	7		
temperature (°C)	70		

Table 3. Diameters and PDI (by DLS) of the Initial Miniemulsion, IMEPP Prior to Purification and G-RNP and G-SNP Redispersed in Various Solvents

sample name		d_n (nm)	d_i (nm)	d_v (nm)	PDI
initial miniemulsion	G-RNP	217	278	305	0.077
	G-SNP	201	224	235	0.037
IMEPP	G-RNP	260	319	365	0.100
	G-SNP	201	232	257	0.061
in toluene	G-RNP	224	285	327	0.153
	G-SNP	170	237	277	0.131
in DMAc	G-RNP	202	285	323	0.112
	G-SNP	195	225	239	0.056
glycocapsules in water	G-RNP	207	290	306	0.105
	G-SNP	164	264	295	0.169

Theoretical calculation[42] of the shell thickness (based on the conversion, contour length, and density of the polymer) indicated that the empty and loaded nanocapsules should have shells with thickness of 17−36 nm. TEM micrographs of all samples showed similar features of hollow core (light) and spherical polymeric shell (dark). From the TEM micrographs (Figure 5 and Figure S3 in the SI), the diameter of the nanocapsules was measured to be 170−236 nm, with a shell thickness of 24−29 nm. These values are well within the theoretically calculated range. DLS analysis indicated the shell thickness of the nanocapsules to be 10−27 nm, calculated from the difference between the d_i of the IMEPP and initial miniemulsion and divided by 2, plus the initial contribution of the PFPMA macroRAFT chain (6 nm) measured from the cryo-TEM (assuming the droplets are directly transformed into the corresponding nanocapsules). The small discrepancy between the two values obtained by DLS and TEM is attributed to the two different states that the measurements were conducted and confirmed the flexibility characteristic of the polymeric shells depending on the environment that they are in.

Production of Glycopolymer Nanocapsules. With the existence of activated ester groups on the shell of the nanocapsules, hydrophilic moieties can be introduced onto the shell via aminolysis. Glucosamine was chosen, not only because of its hydrophilic nature but also due to its biocompatibility.[50] Glycopolymer nanocapsules (glycocapsules) have recently been reported by other techniques using either an emulsion process[51−53] or the use of a sacrificial template.[54] Because fo the low solubility of glucosamine in DMF, the carbohydrate was initially dissolved in water. The addition of the aqueous solution of glucosamine to nanocapsules dispersion in DMF was performed slowly to avoid precipitation. Initial analysis revealed significant leaching (58 wt % in 24 h) of GEM when the loaded nanocapsules were vigorously stirred in water. Leaching was reduced (17 wt % in 24 h) when basic ($NaCO_3$) solution was used to neutralize the drug. Anliker and coworkers[55] previously reported that GEM undergoes degradation under basic conditions; however, the degradation rate was extremely slow with only 28% GEM degraded after 28 days at 40 °C.[55] It can therefore be assumed that after 1 day the deprotonated gemcitabine is stable.

Glucosamine hydrochloride and TEA were both used at a 1:1 molar ratio with respect to the PFPMA group. Equivalent molar ratios were chosen so that the subsequent dialysis process could be completed in the shortest time possible (24 h, against pH 11 water). Similarly, elevated temperature (40 °C) was utilized to increase the reaction rate, with complete conversion obtained in 8 h. After purification, the nanocapsules were readily dispersible in water in contrast with the original hydrophobic

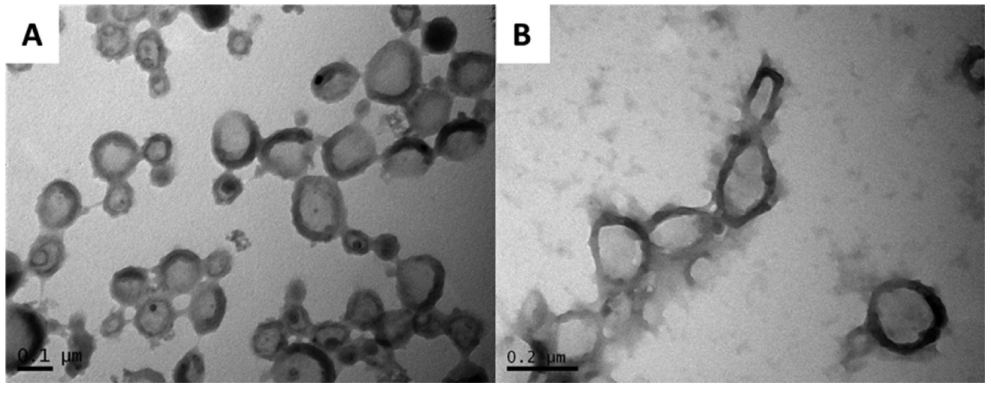

Figure 5. TEM micrographs of loaded nanocapsules (G-RNP, A) and empty nanocapsules (SNP, B) synthesized via IMEPP.

DOI: 10.1021/acs.biomac.5b00545
Biomacromolecules 2015, 16, 2144−2156

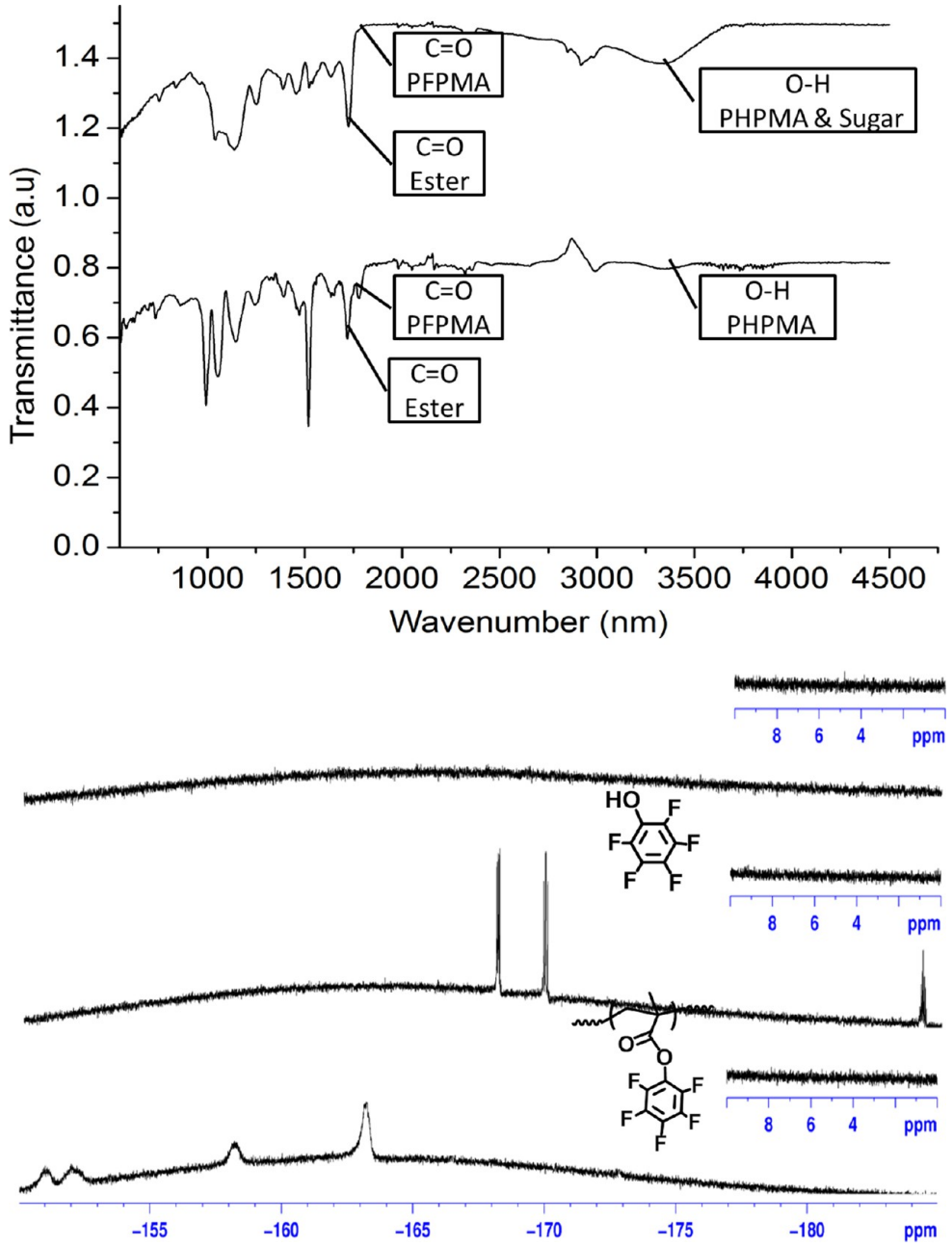

Figure 6. FTIR spectrum (A) of the nanocapsules before (a) and after (b) aminolysis and ^{19}F NMR spectrum (B) of the nanocapsules prior to aminolysis (a), after aminolysis (b) in $CDCl_3$, and after purification (c) in D_2O (corresponding ^{19}F NMR in between 0 and 9 ppm inserted).

nanocapsules. ^{19}F NMR (Figure 6) confirmed the appearance of signals corresponding to pentafluorophenol and the absence of signals relating to PFPMA. Also note that the ^{19}F NMR did not detect any signal corresponding to the gemcitabine (7 ppm). This confirms the absence of any aminolysis reaction between gemcitabine and PFPMA on the shell. FTIR spectra (Figure 6) before and after the reaction also confirmed the disappearance of the activated ester C═O (1779 cm^{-1}) and the pentafluorophenyl (1518 cm^{-1}) peaks as well as the appearance of the broad O−H peak. As previously reported, hydrolysis of the pentafluorophenyl group is suppressed under the similar conditions.[56]

After aminolysis, two representative samples of SNP and G-RNP glyconanocapsules (Glyco-SNP and Glyco-G-RNP, respectively) were further analyzed with DLS and TEM. For the empty nanocapsules, the results confirmed the presence of modified nanocapsules (d_i = 264 nm) of similar size to the initial nanocapsules (d_i = 237 nm, in toluene). No significant increase in particle dispersity was observed, indicating that the aminolysis reaction was not affecting the morphology of the nanocapsules. Similarly, purified loaded nanocapsules redispersed in water had d_i = 290 nm (PDI = 0.105), again comparable to the d_i (285 nm in toluene) prior to the modification. TEM micrographs and analyses (Figure 7 and Figure S3 in the SI) confirmed the size of the nanocapsules to be around 170−240 nm with shell thickness in the range 19−28 nm, similar to before aminolysis.

$^{1}H-^{13}C$ HSQC NMR was carried out on the dispersion (SNP) in D_2O with the aid of cryoprobe to improve the sensitivity. From the ^{1}H NMR (*x*-axis projection, Figure 8), the

DOI: 10.1021/acs.biomac.5b00545
Biomacromolecules 2015, 16, 2144−2156

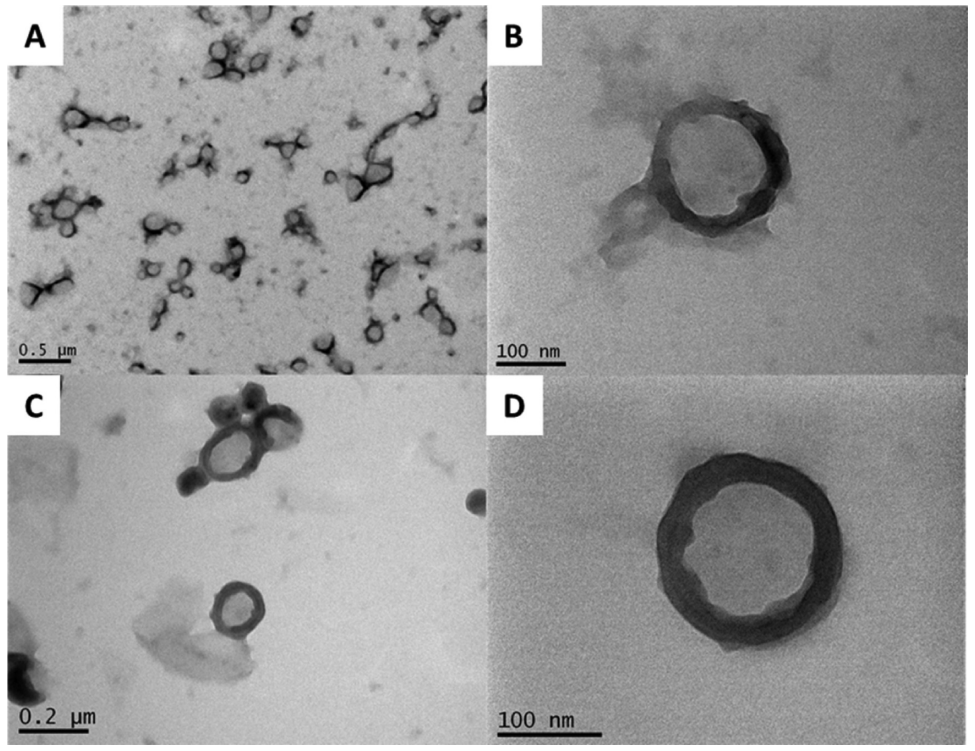

Figure 7. TEM micrographs of the Glyco-SNP (A,B) and Glyco-G-RNP (C,D).

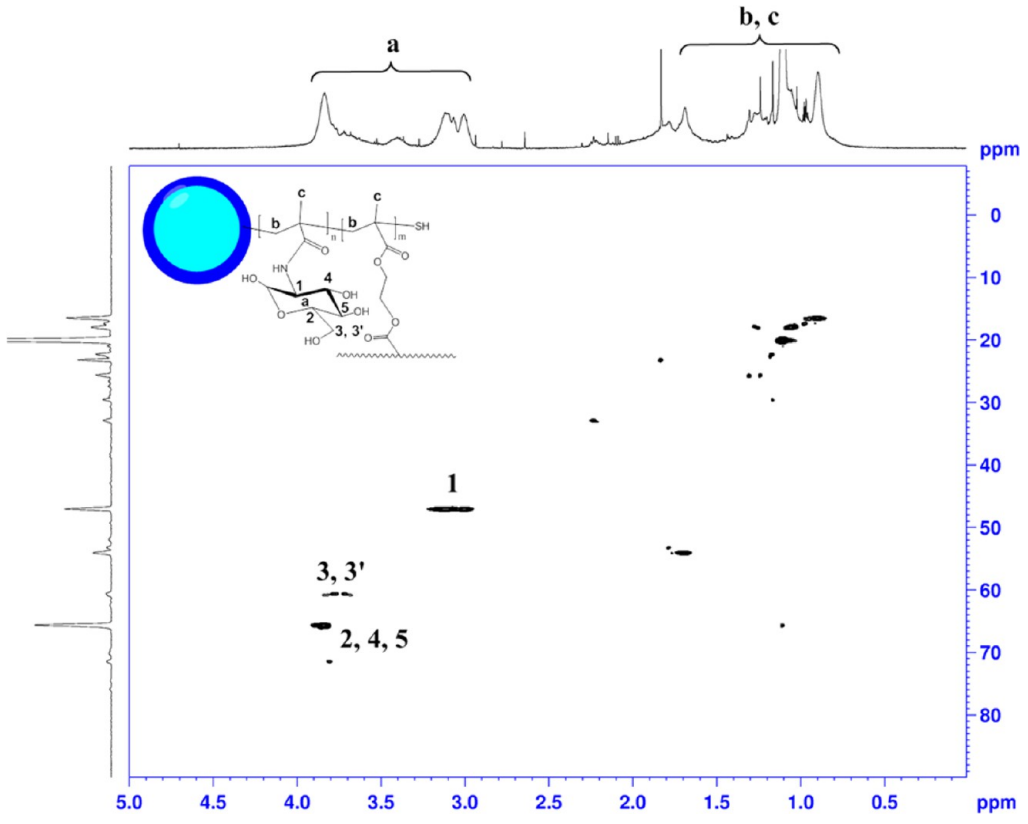

Figure 8. $^{1}H-^{13}C$ HSQC spectrum of the hollow polymeric nanocapsules having glucosamine shells in D_2O.

signals between 3 and 4 ppm (Figure 8a) correspond to protons from the sugar moiety, while the signals between 0.5 and 2 ppm (Figure 8b,c) correspond to protons from the polymeric backbone. These signals were further assigned to their respective ^{13}C signals in the HSQC spectrum (Figure 8). The ^{1}H signals from the sugar moiety (3 to 4 ppm) were individually assigned to the carbon on the sugar ring. The characteristic sugar protons at around 3.6 and 3.9 ppm were

DOI: 10.1021/acs.biomac.5b00545
Biomacromolecules 2015, 16, 2144−2156

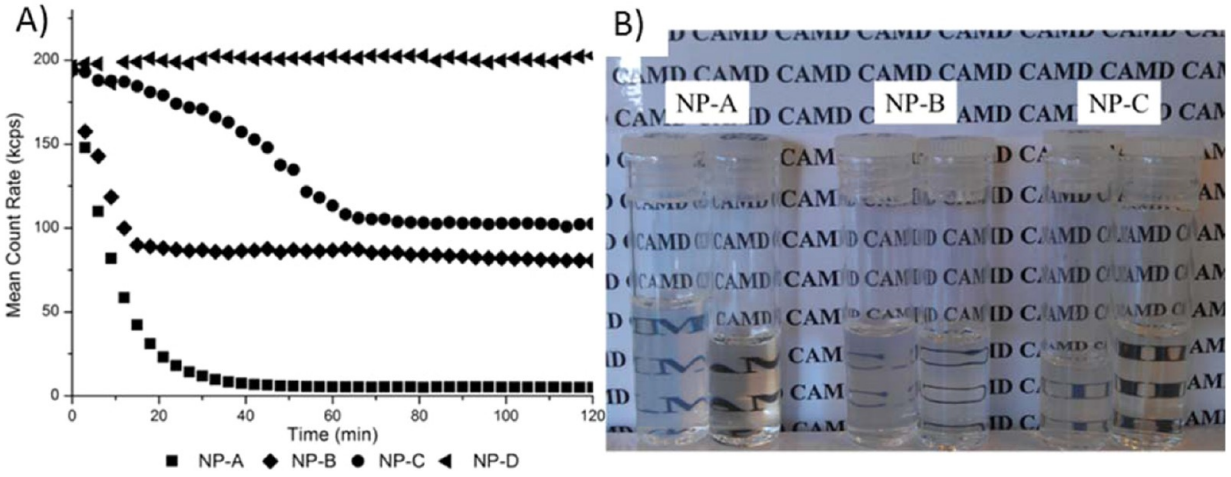

Figure 9. Mean count rate against reaction time plot obtained online using DLS showing the degradation of the nanocapsules (A) and photographs (B) showing the change in turbidity on the solution before (left) and after (right) the reaction.

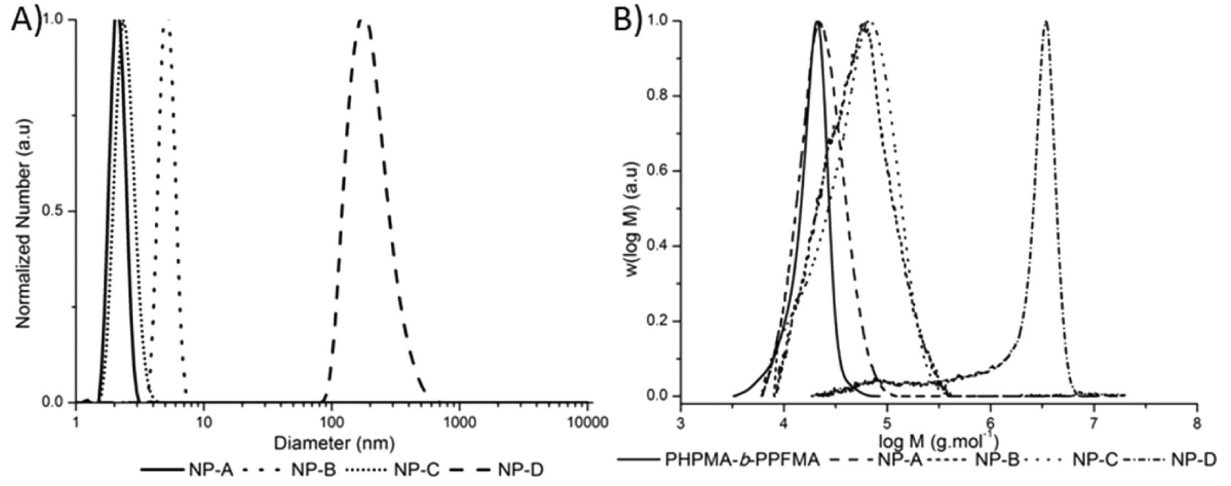

Figure 10. Number-based diameter distributions of the reduced nanocapsules redispersed in DMAc (A) and molecular weight distributions (B) showing the comparison in molecular weight of the cross-linked nanocapsules (dash), the initial block copolymer (solid), and the reduced nanocapsules.

clearly distinguishable as they appeared at the same ^{13}C frequency of around 62 ppm. The broadening of the sugar proton signals indicates the attachment of glucosamine to the polymer. This was also confirmed by testing the spin−lattice relaxation time (T_1), according to which protons attached to larger molecules relax faster than protons attached to small molecules. The sugar protons of the nanocapsules relaxed faster (T_1 = 0.36s) in comparison with those of the PFPMA block copolymer, aminolyzed with glucosamine (T_1 = 0.72s) and the free glucosamine (T_1 = 1.15s).

Degradation of Cross-Linked Nanocapsules via Reduction of Disulfide Group. Disulfide bridges were incorporated into the shell of the nanocapsules to promote a burst-like release of the load once a reductive environment is present. Glutathione in cells is known to reduce disulfide bonds within cytoplasmic proteins, and hence it can also be exploited to reduce the disulfide bonds of the shell. To mimic such a reaction, we exposed loaded nanocapsules to glutathione in water, and the reduction of the disulfide bridge was monitored over time at 40 °C using DLS. Degradation of the cross-links leads to the formation of linear chains that go into solution, thus resulting in disintegration of the nanocapsules.

For comparison, TCEP was also utilized because it has a higher reaction rate than glutathione. For the nanocapsules still having the PFPMA group (NP-A), the reaction was conducted in DMAc, while reaction of nanocapsules with sugar shells (again TCEP and glutathione, NP-B and NP-C, respectively) was conducted in water. Lastly, a control reaction where the reducing agent was omitted (NP-D, in DMAc) was conducted to confirm that the decrease in the DLS count rate was due to the degradation of the shell rather than sedimentation of the nanocapsules over time. Continuous measurements were conducted over 2 h (2 min per measurement with 1 min between measurements).

The control experiment (triangles) clearly showed that the nanocapsules remained stable in DMAc. In contrast, when TCEP (Figure 9, square and diamond) was introduced, the disulfide bond dissociated completely within 25 min. Glutathione (circle) reacted much slower in comparison with TCEP, in which complete reduction was obtained after 60 min. This was confirmed by the drop on the mean count rate to a minimum value and remains stable. This clearly suggested a significant reduction in the size of the object dispersed in the solution (i.e., from nanocapsules to free chain). The reduction

DOI: 10.1021/acs.biomac.5b00545
Biomacromolecules 2015, 16, 2144−2156

Table 4. Summary of the Different Samples That Underwent Reduction Reaction and Their Respective DLS and SEC Data

sample name		reductant (10 mM)	d_n before reduction (nm)	d_n after reduction (nm)	$M_{n,theo}$ (g mol^{-1})	$M_{n,sec}$ (g mol^{-1})
PHPMA-*b*-PPFPMA					11 500	16 200
PPFPMAcapsules	NP-A	TCEP	202	1.94	17 000	18 500
glycocapsules	NP-B	TCEP	207	2.38	16 600	28 300
glycocapsules	NP-C	glutathione	201	7.78	16 600	26 700
glycocapsules	NP-D		206	211		447 800

was also confirmed visually (Figure 9) by the change in the opacity of the solution before and after reaction.

It was noted that for the reduction of the glycocapsules in water (NP-B and NP-C), the count rate did not drop to <5 kcps; instead, it remained stable at ~95 kcps. This behavior was likely caused by the potential aggregation of the free chains in the solution. These solutions were also further analyzed using DLS with an addition of a small quantity of DMAc to break down the aggregation (Figure 10). The results confirmed the presence of free chains (d_n = 8 nm) for NP-B and NP-C (d_n = 2 nm). The presence of free chains was also confirmed by SEC (Figure 10), whereby the molecular weights of the products from the reduction reaction were found to be significantly lower than that of the initial cross-linked nanocapsules (Table 4).

Quantification of the Encapsulated Gemcitabine and Its Release via HPLC. Initially, an HPLC calibration curve of gemcitabine at various concentrations was constructed (Figure S4 in the SI). The release of gemcitabine under basic condition was investigated by having G-RNP prior to aminolysis vigorously stirred in basic water (1 mg/mL, pH 11) for 6, 12, 24, and 48 h. The rate of release was found to be low under these conditions, although some GEM was released within the first 12 h. This was attributed to the some GEM being encapsulated close or within the shell, which allows the quick release. Over time, the release rate significantly decreased before ceasing after 24 h. The experiment was carried out for a further 24 h to confirm the absence of diffusion release afterward. The wt % of GEM released during this stage was 17 wt % (Figure 11). This indicates that during the purification of glycocapsules (via dialysis under the same condition), 17 wt % of GEM was lost.

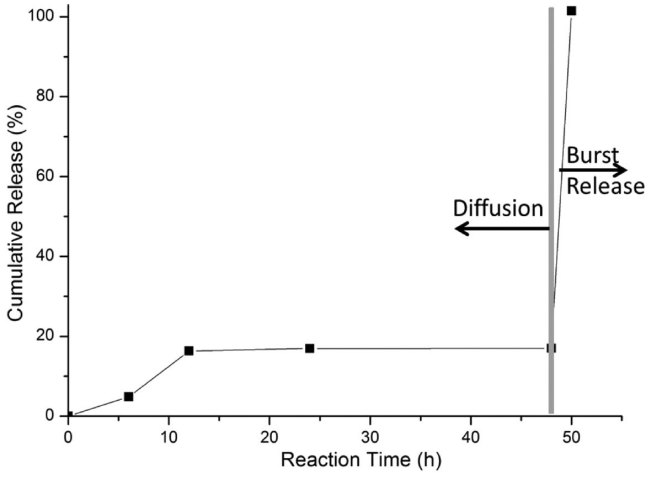

Figure 11. GEM cumulative release showing the diffusion-controlled release for 48 h and the burst release after the addition of glutathione (10 mM).

The glycopolymer nanocapsules (1 mg/mL) were reacted with glutathione in water for 1 h to promote the reduction of the disulfide bond. Simultaneously, a burst-like release of the drug was observed. The result indicated that 104 μg/mg or 84.5 wt % of GEM was released in <2 h. The structural integrity of GEM was confirmed during the HPLC analysis previously. It was shown by the absence of any shift on the retention time between the pure GEM and the GEM released from the nanocapsules (Figure S5 in the SI).

Cytotoxicity Study against Pancreatic Cancer Cell Lines. GEM-loaded nanocapsules were tested against human pancreatic cancer (AsPC-1) to test its efficacy in comparison with the free GEM drug. First of all, the toxicity of the hollow nanocapsules (RNP) without drug was tested against the cell lines. The result showed that the nanocapsules were not toxic, as indicated by the 100% cell viability obtained from the solution with nanocapsules concentration of up to 200 μg/mL.

The cytotoxicity of GEM loaded-nanocapsules was evaluated and compared with that of the free GEM to test the efficacy of the synthesized nanocapsules as a drug carrier. Pure GEM (GEM·HCl, 10 μM) and GEM loaded in permanently cross-linked and reducible nanocapsules (G-SNP and G-RNP respectively, [NPs] = 28.9 μg/mL, [GEM] = 10 μM) were compared (Figure 12). The cell viability was then plotted

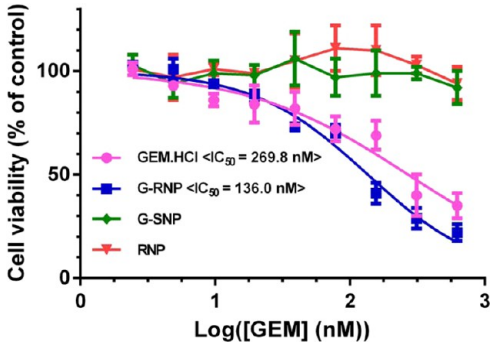

Figure 12. Cytotoxicity study result of the hollow nanocapsules (RNP), free GEM (GEM·HCl), GEM-nanocapsules with a reducible shell (G-RNP), and GEM nanocapsules with a solid shell (G-SNP).

against the GEM concentration to evaluate the role of nanocapsules in improving the cytotoxicity. Furthermore, both G-SNP and G-RNP were tested to evaluate the effect of the reducible shell on the toxicity.

The IC_{50} value of GEM alone was found to be ~270 nM. When nanocapsules with reducible shell were used, the cytotoxicity of GEM was found to increase by 2-fold, resulting in an IC_{50} value of 136 nM. The increase in toxicity on the loaded nanocapsules is attributed to the prolonged bioavailability and the higher cellular accumulation of the nanocapsules within the tumor cells.[57−59] Promoted by these factors, the accumulation of drug within the tumor cells was higher than that of the free GEM. Furthermore, the result for G-SNP

DOI: 10.1021/acs.biomac.5b00545
Biomacromolecules 2015, 16, 2144−2156

showed no toxicity (~97% cell viability) against the cell lines. This, first of all, indicates that the shell was able to protect the load from being released prematurely. Second, when compared with the result of G-RNP, the predominant release mechanism can be safely associated with the reduction of the shell by glutathione and not the diffusion of the drug through the pores of the shell.

CONCLUSIONS

Nanocapsules having reactive functionalities on the shell were successfully synthesized using the versatile IMEPP process. Amphiphilic RAFT block copolymer was visually confirmed to be able to stabilize the inverse miniemulsion in the absence of any surfactants. The IMEPP mechanism itself was extensively studied. The results indicated that the shell grew in accordance to the polymerization rate and the thickness could be tuned efficiently by stopping the polymerization at the desired thickness. The resulting nanocapsules were also found to be comparable to the initial droplets, in terms of their size and their dispersity. The core−shell morphology of the nanocapsules was also confirmed via TEM. The capability of the nanocapsules to be postmodified was shown by the successful decoration of the shell with sugar moieties. This not only changes the polarity of the nanocapsules but also makes them noncytotoxic.

The suitability of the nanocapsules as a drug carrier was confirmed, and their potential application as a drug carrier was reported herein. First of all, because the drug came in a salt form, its suitability to completely substitute NaCl as the lipophobe was confirmed, with no significant changes on the size and stability of the miniemulsion observed. Subsequently, the loaded nanocapsules were synthesized in a one-pot process, with the resulting products cross-linked by the bioreducible, disulfide linker. The loaded nanocapsules were further modified to make it biocompatible, with little loss of the load during the process. Using this approach, an EE of ~100% and loading efficiency of ~11% were achieved. Against pancreatic cancer cell lines, the nanocapsules were able to improve the cytotoxicity of the drug by 2-fold.

ASSOCIATED CONTENT

Supporting Information

^{1}H and ^{19}F NMR of the polymers, DLS distributions plot for RNP and G-RNP, HPLC calibration curve for gemcitabine, and HPLC chromatograms for both native and encapsulated gemcitabine. The Supporting Information is available free of charge on the ACS Publications website at DOI: 10.1021/acs.biomac.5b00545.

AUTHOR INFORMATION

Corresponding Authors

*(P.B.Z.) E-mail: p.zetterlund@unsw.edu.au.
*(M.H.S.) E-mail: m.stenzel@unsw.edu.au.

Notes

The authors declare no competing financial interest.

ACKNOWLEDGMENTS

R.H.U. is grateful for a student exchange scholarship from UNSW student exchange office. R.H.U. thanks UNSW Mark Wainwright Analytical Centre for the NMR analyses and Dr. Markus Drechsler from BIMF at Universität Bayreuth for the cryo-TEM images. M.S. and P.Z. acknowledge the Australian Research Council (ARC) for funding.

REFERENCES

(1) Mora-Huertas, C. E.; Fessi, H.; Elaissari, A. *Int. J. Pharm.* **2010**, *385*, 113.
(2) Soppimath, K. S.; Aminabhavi, T. M.; Kulkarni, A. R.; Rudzinski, W. E. *J. Controlled Release* **2001**, *70*, 1.
(3) Jain, R. K.; Stylianopoulos, T. *Nat. Rev. Clin. Oncol.* **2010**, *7*, 653.
(4) Petros, R. A.; DeSimone, J. M. *Nat. Rev. Drug Discovery* **2010**, *9*, 615.
(5) Allen, T. M.; Cullis, P. R. *Adv. Drug Delivery Rev.* **2013**, *65*, 36.
(6) Karagoz, B.; Boyer, C.; Davis, T. P. *Macromol. Rapid Commun.* **2014**, *35*, 417.
(7) Chen, Y.; Chen, H.; Zeng, D.; Tian, Y.; Chen, F.; Feng, J.; Shi, J. *ACS Nano* **2010**, *4*, 6001.
(8) Gu, X.; Wang, J.; Wang, Y.; Wang, Y.; Gao, H.; Wu, G. *Colloids Surf., B* **2013**, *108*, 205.
(9) Du, A. W.; Stenzel, M. H. *Biomacromolecules* **2014**, *15*, 1097.
(10) Immordino, M. L.; Brusa, P.; Rocco, F.; Arpicco, S.; Ceruti, M.; Cattel, L. *J. Controlled Release* **2004**, *100*, 331.
(11) Vandana, M.; Sahoo, S. K. *Biomaterials* **2010**, *31*, 9340.
(12) Yang, J.; Luo, K.; Pan, H.; Kopečková, P.; Kopeček, J. *React. Funct. Polym.* **2011**, *71*, 294.
(13) Cavallaro, G.; Mariano, L.; Salmaso, S.; Caliceti, P.; Gaetano, G. *Int. J. Pharm.* **2006**, *307*, 258.
(14) Yang, Z.; Lee, J. H.; Jeon, H. M.; Han, J. H.; Park, N.; He, Y.; Lee, H.; Hong, K. S.; Kang, C.; Kim, J. S. *J. Am. Chem. Soc.* **2013**, *135*, 11657.
(15) Chitkara, D.; Mittal, A.; Behrman, S. W.; Kumar, N.; Mahato, R. I. *Bioconjugate Chem.* **2013**, *24*, 1161.
(16) Mittal, A.; Chitkara, D.; Behrman, S. W.; Mahato, R. I. *Biomaterials* **2014**, *35*, 7077.
(17) Bornmann, C.; Graeser, R.; Esser, N.; Ziroli, V.; Jantscheff, P.; Keck, T.; Unger, C.; Hopt, U. T.; Adam, U.; Schaechtele, C.; Massing, U.; von Dobschuetz, E. *Cancer Chemother. Pharmacol.* **2008**, *61*, 395.
(18) Yang, J.; Park, S. B.; Yoon, H.-G.; Huh, Y. M.; Haam, S. *Int. J. Pharm.* **2006**, *324*, 185.
(19) Arias, J. L.; Reddy, L. H.; Couvreur, P. *J. Drug Targeting* **2009**, *17*, 586.
(20) Celia, C.; Malara, N.; Terracciano, R.; Cosco, D.; Paolino, D.; Fresta, M.; Savino, R. *Nanomed. Nanotechnol. Biol. Med.* **2008**, *4*, 155.
(21) Grazia Calvagno, M.; Celia, C.; Paolino, D.; Cosco, D.; Iannone, M.; Castelli, F.; Doldo, P.; Fresta, M. *Curr. Drug Delivery* **2007**, *4*, 89.
(22) Celia, C.; Cosco, D.; Paolino, D.; Fresta, M. *Expert Opin. Drug Delivery* **2011**, *8*, 1609.
(23) Wang, Y.; Fan, W.; Dai, X.; Katragadda, U.; McKinley, D.; Teng, Q.; Tan, C. *Mol. Pharmaceutics* **2014**, *11*, 1140.
(24) Zhu, S.; Lansakara-P, D. S.; Li, X.; Cui, Z. *Bioconjugate Chem.* **2012**, *23*, 966.
(25) Arpicco, S.; Lerda, C.; Dalla Pozza, E.; Costanzo, C.; Tsapis, N.; Stella, B.; Donadelli, M.; Dando, I.; Fattal, E.; Cattel, L.; Palmieri, M. *Eur. J. Pharm. Biopharm.* **2013**, *85*, 373.
(26) Chitkara, D.; Mittal, A.; Behrman, S. W.; Kumar, N.; Mahato, R. I. *Bioconjugate Chem.* **2013**, *24*, 1161.
(27) Wang, W.; Li, C.; Zhang, J.; Dong, A.; Kong, D. *J. Mater. Chem. B* **2014**, *2*, 1891.
(28) Delplace, V.; Couvreur, P.; Nicolas, J. *Polym. Chem.* **2014**, *5*, 1529.
(29) Duc Trung, B.; Maksimenko, A.; Desmaele, D.; Harrisson, S.; Vauthier, C.; Couvreur, P.; Nicolas, J. *Biomacromolecules* **2013**, *14*, 2837.
(30) Harrisson, S.; Nicolas, J.; Maksimenko, A.; Duc Trung, B.; Mougin, J.; Couvreur, P. *Angew. Chem., Int. Ed.* **2013**, *52*, 1678.
(31) Maksimenko, A.; Bui, D. T.; Desmaele, D.; Couvreur, P.; Nicolas, J. *Chem. Mater.* **2014**, *26*, 3606.
(32) Baier, G.; Musyanovych, A.; Dass, M.; Theisinger, S.; Landfester, K. *Biomacromolecules* **2010**, *11*, 960.

DOI: 10.1021/acs.biomac.5b00545
Biomacromolecules 2015, 16, 2144−2156

(33) Fang, J.-H.; Lai, Y.-H.; Chiu, T.-L.; Chen, Y.-Y.; Hu, S.-H.; Chen, S.-Y. *Adv. Healthcare Mater.* **2014**, *8*, 1250.
(34) Jain, A. K.; Thanki, K.; Jain, S. *Mol. Pharmaceutics* **2013**, *10*, 3459.
(35) Li, W.; Matyjaszewski, K.; Albrecht, K.; Möller, M. *Macromolecules* **2009**, *42*, 8228.
(36) Li, W.; Yoon, J. A.; Matyjaszewski, K. *J. Am. Chem. Soc.* **2010**, *132*, 7823.
(37) Lu, F.; Luo, Y.; Li, B. *Ind. Eng. Chem. Res.* **2010**, *49*, 2206.
(38) Lu, F.; Luo, Y.; Li, B.; Zhao, Q.; Schork, F. J. *Macromolecules* **2009**, *43*, 568.
(39) Luo, Y.; Gu, H. *Polymer* **2007**, *48*, 3262.
(40) Shirin-Abadi, A. R.; Mahdavian, A. R.; Khoee, S. *Macromolecules* **2011**, *44*, 7405.
(41) Paiphansiri, U.; Dausend, J.; Musyanovych, A.; Mailänder, V.; Landfester, K. *Macromol. Biosci.* **2009**, *9*, 575.
(42) Utama, R. H.; Stenzel, M. H.; Zetterlund, P. B. *Macromolecules* **2013**, *46*, 2118.
(43) Utama, R. H.; Drechsler, M.; Förster, S.; Zetterlund, P. B.; Stenzel, M. H. *ACS Macro Lett.* **2014**, *3*, 935.
(44) Utama, R. H.; Dulle, M.; Förster, S.; Stenzel, M. H.; Zetterlund, P. B. *Macromol. Rapid Commun.* **2015**, n/a.
(45) Utama, R. H.; Guo, Y.; Zetterlund, P. B.; Stenzel, M. H. *Chem. Commun.* **2012**, *48*, 11103.
(46) Paolino, D.; Cosco, D.; Celano, M.; Moretti, S.; Puxeddu, E.; Russo, D.; Fresta, M. *Nanomedicine* **2013**, *8*, 193.
(47) Mitsukami, Y.; Donovan, M. S.; Lowe, A. B.; McCormick, C. L. *Macromolecules* **2001**, *34*, 2248.
(48) Tucker, B. S.; Sumerlin, B. S. *Polym. Chem.* **2014**, *5*, 1566.
(49) Taylor, P. *Adv. Colloid Interface Sci.* **1998**, *75*, 107.
(50) Ting, S. R. S.; Chen, G.; Stenzel, M. H. *Polym. Chem.* **2010**, *1*, 1392.
(51) Roux, R.; Sallet, L.; Alcouffe, P.; Chambert, S.; Sintes-Zydowicz, N.; Fleury, E.; Bernard, J. *ACS Macro Lett.* **2012**, *1*, 1074.
(52) Freichels, H.; Wagner, M.; Okwieka, P.; Meyer, R. G.; Mailander, V.; Landfester, K.; Musyanovych, A. *J. Mater. Chem. B* **2013**, *1*, 4338.
(53) Yan, X.; Delgado, M.; Fu, A.; Alcouffe, P.; Gouin, S. G.; Fleury, E.; Katz, J. L.; Ganachaud, F.; Bernard, J. *Angew. Chem., Int. Ed.* **2014**, *53*, 6910.
(54) Ting, S. R. S.; Gregory, A. M.; Stenzel, M. H. *Biomacromolecules* **2009**, *10*, 342.
(55) Anliker, S. L.; McClure, M. S.; Britton, T. C.; Stephan, E. A.; Maple, S. R.; Cooke, G. G. *J. Pharm. Sci.* **1994**, *83*, 716.
(56) Boyer, C.; Davis, T. P. *Chem. Commun.* **2009**, 6029.
(57) Kim, Y.; Pourgholami, M. H.; Morris, D. L.; Lu, H.; Stenzel, M. H. *Biomater. Sci.* **2013**, *1*, 265.
(58) Kim, Y.; Pourgholami, M. H.; Morris, D. L.; Stenzel, M. H. *Biomacromolecules* **2012**, *13*, 814.
(59) Lu, H.; Utama, R. H.; Kitiyotsawat, U.; Babiuch, K.; Jiang, Y.; Stenzel, M. H. *Biomater. Sci.* **2015**, DOI: 10.1039/C4BM00323C.

DOI: 10.1021/acs.biomac.5b00545
Biomacromolecules 2015, 16, 2144−2156